

# Causal Explanations for Image Classifiers

Hana Chockler and David A. Kelly and Daniel Kroening and Youcheng Sun

King's College London

Amazon.com, Inc.

Mohamed bin Zayed University of Artificial Intelligence and University of Manchester

## Abstract

Existing algorithms for explaining the output of image classifiers use different definitions of explanations and a variety of techniques to extract them. However, none of the existing tools use a principled approach based on formal definitions of causes and explanations for the explanation extraction.

In this paper we present a novel black-box approach to computing explanations grounded in the theory of actual causality. We prove relevant theoretical results and present an algorithm for computing approximate explanations based on these definitions. We prove termination of our algorithm and discuss its complexity and the amount of approximation compared to the precise definition.

We implemented the framework in a tool ReX and we present experimental results and a comparison with state-of-the-art tools. We demonstrate that ReX is the most efficient tool and produces the smallest explanations, in addition to outperforming other black-box tools on standard quality measures.

## 1 Introduction

Neural networks (NNs) are now a primary building block of many computer vision systems. NNs are complex non-linear functions with algorithmically generated (and not engineered) coefficients. In contrast to traditionally engineered image processing pipelines it is difficult to retrace how the pixel data are interpreted by the layers of the network. Moreover, in many application areas, in particular healthcare, the networks are proprietary, making the analysis of the internal layers impossible. This “black box” nature of neural networks creates demand for techniques that explain why a particular input yields the output that is observed without understanding the model’s parameters and their influence on the output.

An explanation of an output of an automated procedure is essential in many areas, including verification, planning, diagnosis and the like. A good explanation can increase a user’s confidence in the result. Explanations are also useful for determining whether there is a fault in the automated procedure: if the explanation does not make sense, it may indicate that the procedure is faulty. It is less clear how to define what a *good* explanation is. There have been a number

of definitions of explanations over the years in various domains of computer science (Chajewska and Halpern 1997; Gärdenfors 1988; Pearl 1988), philosophy (Hempel 1965) and statistics (Salmon 1989).

Black-box explanations for the results of image classifiers are typically based on or are given in the form of a *ranking* of the pixels, which is a numerical measure of importance: the higher the score, the more important the pixel is for the NN’s classification outcome. Often these rankings are presented in a form of a *heat map*, with higher scores corresponding to hotter areas. A user-friendly explanation can then be a subset of highest-ranked pixels that is sufficient for the original classification outcome.

This paper addresses the following research questions:

- RQ1** What is a formal rigorous definition of explanation, suitable for image classification?
- RQ2** Can we compute explanations based on the definition above without opening the black box? What is the complexity of such computation?
- RQ3** Is there an efficiently computable approximation to explanations?
- RQ4** What are suitable quality measures for explanations? A measure is suitable if it is meaningful with respect to quality and produces results that match our intuition.
- RQ5** What is the quality of explanations computed by our algorithms compared to other black-box methods?
- RQ6** Is there a trade-off between quality and compute cost of the explanations?
- RQ7** Can black-box methods achieve the same quality of explanations as white-box methods?

Our algorithms are based on the formal definition of explanation in the theory of actual causality by (Halpern 2019) and its adaptation to image classifiers by (Chockler and Halpern 2024). Essentially, an explanation in the context of image classifiers is a minimal subset of pixels and their values in the original image that is sufficient for obtaining the same classification as the original image, given that the rest of the image has value taken from a predefined dataset. We view the NN as a causal model of depth two, with the classification computed in one internal node, thus capturing the opacity of the network. The algorithm then calculates an

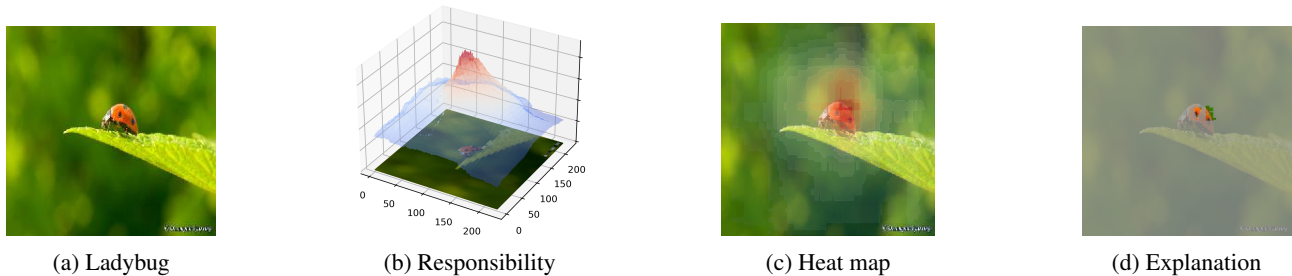


Figure 1: A ladybug (a), its responsibility map (b), the heat map (c), which is a projection of the responsibility map on a plane overlaid on the original image, and a causal explanation (d). The minimal causal explanation computed by our tool ReX is just 0.03% of the image.

approximate explanation, where the approximation is in the size of the explanation. That is, an explanation computed by our algorithm is sufficient for the classification, but it might not be minimal, though it is very close to minimal on real images: in our experiments, the average size of an explanation is  $\approx 5\%$  of the image, which is smaller than any of the other black-box tools and is likely to be close to minimal from the human perspective. We formally prove termination and complexity of our algorithm and discuss its approximation ratio.

We compare the experimental results of our implementation of the algorithm in a tool ReX with those of other black-box tools on a number of benchmark datasets: ImageNet, VOC2012, and a set of partially occluded images. Our results show that ReX is on par with the most efficient tools in terms of execution time, while producing the smallest explanations. We also analyse the explanations using the standard measures of insertion and deletion curves and the intersection with the background or the occlusion. The results show that ReX outperforms the other tools on insertion curves and the overlap with irrelevant parts of the image. We discuss the logic behind deletion curves and demonstrate that low deletion is a measure of the quality of the model for particular types of images, rather than for the quality of an explanation. We also argue that explanations computed by ReX are so small that any further reduction in their size is meaningless.

The rest of the paper is organized as follows. Section 2 presents an overview of the related work on black-box explainable AI. Section 3 gives the necessary background on actual causality. Section 4 provides the theoretical foundations of our approach to explainability. Section 5 is a detailed overview of our algorithm, with the evaluation results discussed in Section 6. The tool ReX is open source and available at <https://github.com/ReX-XAI/ReX>. All benchmark sets are publicly available and referenced in Section 6.

## 2 Related Work

There is a large body of work on explaining the results of image classifiers. As our primary interest is in black-box approaches, we only give a brief overview of the white-box algorithms here. The existing approaches to *post hoc*

explainability can be largely grouped into two categories: propagation and perturbation.

Propagation-based explanation methods are often regarded as more efficient. They back-propagate a model’s decision to the input layer to determine the weight of each input feature for the decision. GRAD-CAM by (Selvaraju et al. 2017) only needs one backward pass and propagates the class-specific gradient into the final convolutional layer of a DNN to coarsely highlight important regions of an input image. Guided Back-Propagation (GBP) by (Springenberg et al. 2015) computes the single and average partial derivatives of the output to attribute the prediction of a DNN. Integrated Gradients (IG) by (Sundararajan, Taly, and Yan 2017) further uses two axioms called sensitivity and completeness for the problem of how to attribute the classification by a deep network to its input features. NoiseTunnel by (Adebayo et al. 2018) adds gaussian noise to the image before applying another XAI method. The noise serves to smooth any resultant saliency map, improving explanation quality. SHAP (SHapley Additive exPlanations) by (Lundberg and Lee 2017a) goes beyond propagation and identifies inputs that are similar to the input for which the output is to be explained, and ranks the features of the input according to their difference. A key advantage of SHAP is that it does not require counterfactuals. GradientSHAP is gradient-based method that approximates Shapley values via gradient integration and a noise tunnel. Both IG and GradientSHAP require access to model gradients while computing explanations. They form part of a family of whitebox explanation methods which differ from the GRAD-CAM family in that they do not rely on examination of specified activation layers in the model. Other methods for approximating Shapley values are numerous, among which KERNELSHAP (Lundberg and Lee 2017a) and DEEPLIFTSHAP (Lundberg and Lee 2017a) are probably the most used. KERNELSHAP uses the LIME framework to approximate Shapley values, whereas DEEPLIFTSHAP uses the DEEPLIFT (Shrikumar, Greenside, and Kundaje 2017) method to the same end.

In contrast to propagation-based explanation methods, perturbation-based explanation approaches explore the input space directly in search for an explanation. The exploration/search often requires a large number of inference passes, which incurs significant computational cost when compared to propagation methods. There are many sam-

pling methods, most of which are based on random search or heuristics. The chief advantage of perturbation-based methods is that they are model independent and do not require any access to model internals. Given a particular input, LIME by (Ribeiro, Singh, and Guestrin 2016) samples the neighborhood of this input and creates an inherently explainable model to approximate the system’s local behavior; owing to the high computational cost of this approach, the ranking uses super-pixels via segmentation instead of individual pixels. (Datta, Sen, and Zick 2016) replace the natural distribution of the input by a user-defined distribution and then use the Shapley Value method to analyze combinations of input features and to rank their importance. (Chen et al. 2018) estimate the importance of input features by measuring the flow of information between inputs and outputs. Both the Shapley Value and the information-theoretic approaches are computationally expensive. In RISE by (Petsiuk, Das, and Saenko 2018), the importance of a pixel is computed as the expectation over all local perturbations conditioned on the event that the pixel is observed. (Fong, Patrick, and Vedaldi 2019) have introduced the concept of “extreme perturbations” to improve the perturbation analysis in the EXTREMAL algorithm. More recently, spectrum-based fault localisation (SBFL) has been applied to explaining image classifiers. The technique has been implemented in the tool DeepCover by (Sun et al. 2020).

The method and tool, ReX, presented in this paper is a perturbation-based approach and addresses the limitations of existing black-box methods in two aspects. The feature masking in ReX uses causal reasoning that provides a guarantee (subject to the assumption). Owing to its guided iterative refinement, ReX is computationally efficient, while still producing explanations that are the state of the art.

### 3 Background on Actual Causality

In this section, we briefly review the definitions of causality and causal models introduced by (Halpern and Pearl 2005a) and relevant definitions of causes and explanations in image classification by (Chockler and Halpern 2024). The reader is referred to (Halpern 2019) for further reading.

We assume that the world is described in terms of variables and their values. Some variables may have a causal influence on others. This influence is modeled by a set of *structural equations*. It is conceptually useful to split the variables into two sets: the *exogenous* variables, whose values are determined by factors outside the model, and the *endogenous* variables, whose values are ultimately determined by the exogenous variables. The structural equations describe how these values are determined.

Formally, a *causal model*  $M$  is a pair  $(\mathcal{S}, \mathcal{F})$ , where  $\mathcal{S}$  is a *signature*, which explicitly lists the endogenous and exogenous variables and characterizes their possible values, and  $\mathcal{F}$  defines a set of (*modifiable*) *structural equations*, relating the values of the variables. A signature  $\mathcal{S}$  is a tuple  $(\mathcal{U}, \mathcal{V}, \mathcal{R})$ , where  $\mathcal{U}$  is a set of exogenous variables,  $\mathcal{V}$  is a set of endogenous variables, and  $\mathcal{R}$  associates with every variable  $Y \in \mathcal{U} \cup \mathcal{V}$  a nonempty set  $\mathcal{R}(Y)$  of possible values for  $Y$  (i.e., the set of values over which  $Y$  ranges). For simplicity, we assume here that  $\mathcal{V}$  is finite,

as is  $\mathcal{R}(Y)$  for every endogenous variable  $Y \in \mathcal{V}$ . The set  $\mathcal{F}$  associates with each endogenous variable  $X \in \mathcal{V}$  a function denoted  $F_X$  (i.e.,  $F_X = \mathcal{F}(X)$ ) such that  $F_X : (\times_{U \in \mathcal{U}} \mathcal{R}(U)) \times (\times_{Y \in \mathcal{V} - \{X\}} \mathcal{R}(Y)) \rightarrow \mathcal{R}(X)$ .

The structural equations define what happens in the presence of external interventions. Setting the value of some variable  $X$  to  $x$  in a causal model  $M = (\mathcal{S}, \mathcal{F})$  results in a new causal model, denoted  $M_{X \leftarrow x}$ , which is identical to  $M$ , except that the equation for  $X$  in  $\mathcal{F}$  is replaced by  $X = x$ .

*Probabilistic causal models* are pairs  $(M, \text{Pr})$ , where  $M$  is a causal model and  $\text{Pr}$  is a probability on the contexts. A causal model  $M$  is *recursive* (or *acyclic*) if its causal graph is acyclic. If  $M$  is an acyclic causal model, then given a *context*, that is, a setting  $\vec{u}$  for the exogenous variables in  $\mathcal{U}$ , the values of all the other variables are determined. In this paper we restrict the discussion to recursive models.

We call a pair  $(M, \vec{u})$  consisting of a causal model  $M$  and a context  $\vec{u}$  a (*causal*) *setting*. A causal formula  $\psi$  is true or false in a setting. We write  $(M, \vec{u}) \models \psi$  if the causal formula  $\psi$  is true in the setting  $(M, \vec{u})$ . The  $\models$  relation is defined inductively.  $(M, \vec{u}) \models X = x$  if the variable  $X$  has value  $x$  in the unique solution to the equations in  $M$  in context  $\vec{u}$ . Finally,  $(M, \vec{u}) \models [\vec{Y} \leftarrow \vec{y}] \varphi$  if  $(M_{\vec{Y} \leftarrow \vec{y}}, \vec{u}) \models \varphi$ , where  $M_{\vec{Y} \leftarrow \vec{y}}$  is the causal model that is identical to  $M$ , except that the variables in  $\vec{Y}$  are set to  $Y = y$  for each  $Y \in \vec{Y}$  and its corresponding value  $y \in \vec{y}$ .

A standard use of causal models is to define *actual causation*: that is, what it means for some particular event that occurred to cause another particular event. There have been a number of definitions of actual causation given for acyclic models (e.g., (Beckers 2021; Glymour and Wimberly 2007; Hall 2007; Halpern and Pearl 2005a; Halpern 2019; Hitchcock 2001; 2007; Weslake 2015; Woodward 2003)). In this paper, we focus on what has become known as the *modified Halpern–Pearl* definition and some related definitions introduced by (Halpern 2019). We briefly review the relevant definitions below. The events that can be causes are arbitrary conjunctions of primitive events (formulas of the form  $X = x$ ); the events that can be caused are primitive events, denoting the output of the model.

**Definition 3.1** (Actual cause).  $\vec{X} = \vec{x}$  is an *actual cause* of  $\varphi$  in  $(M, \vec{u})$  if the following three conditions hold:

- AC1.  $(M, \vec{u}) \models (\vec{X} = \vec{x})$  and  $(M, \vec{u}) \models \varphi$ .
- AC2. There is a setting  $\vec{x}'$  of the variables in  $\vec{X}$ , a (possibly empty) set  $\vec{W}$  of variables in  $\mathcal{V} - \vec{X}'$ , and a setting  $\vec{w}$  of the variables in  $\vec{W}$  such that  $(M, \vec{u}) \models \vec{W} = \vec{w}$  and  $(M, \vec{u}) \models [\vec{X} \leftarrow \vec{x}', \vec{W} \leftarrow \vec{w}] \neg \varphi$ , and moreover
- AC3.  $\vec{X}$  is minimal; there is no strict subset  $\vec{X}'$  of  $\vec{X}$  such that  $\vec{X}' = \vec{x}''$  can replace  $\vec{X} = \vec{x}'$  in AC2, where  $\vec{x}''$  is the restriction of  $\vec{x}'$  to the variables in  $\vec{X}'$ .

In the special case that  $\vec{W} = \emptyset$ , we get the but-for definition. A variable  $x$  in an actual cause  $\vec{X}$  is called a *part of a cause*. In what follows, we adopt the convention of Halpern and state that *part of a cause is a cause*.

The notion of explanation taken from (Halpern 2019) is relative to a set of contexts.

**Definition 3.2** (Explanation).  $\vec{X} = \vec{x}$  is an *explanation* of  $\varphi$  relative to a set  $\mathcal{K}$  of contexts in a causal model  $M$  if the following conditions hold:

EX1a. If  $\vec{u} \in \mathcal{K}$  and  $(M, \vec{u}) \models (\vec{X} = \vec{x}) \wedge \varphi$ , then there exists a conjunct  $X = x$  of  $\vec{X} = \vec{x}$  and a (possibly empty) conjunction  $\vec{Y} = \vec{y}$  such that  $X = x \wedge \vec{Y} = \vec{y}$  is an actual cause of  $\varphi$  in  $(M, \vec{u})$ .

EX1b.  $(M, \vec{u}') \models [\vec{X} = \vec{x}] \varphi$  for all contexts  $\vec{u}' \in \mathcal{K}$ .

EX2.  $\vec{X}$  is minimal; there is no strict subset  $\vec{X}'$  of  $\vec{X}$  such that  $\vec{X}' = \vec{x}'$  satisfies EX1, where  $\vec{x}'$  is the restriction of  $\vec{x}$  to the variables in  $\vec{X}'$ . (This is SC4).

EX3.  $(M, u) \models \vec{X} = \vec{x} \wedge \varphi$  for some  $u \in \mathcal{K}$ .

## 4 Theoretical Foundations

We approach the first two research questions theoretically.

**RQ1** What is a formal rigorous definition of explanation, suitable for image classification?

We view an image classifier (*e.g.* a neural network) as a probabilistic causal model. Specifically, the endogenous variables are taken to be the set  $\vec{V}$  of pixels that the image classifier gets as input, together with an output variable that we call  $O$ . The variable  $V_i \in \vec{V}$  describes the color and intensity of pixel  $i$ ; its value is determined by the exogenous variables. The equation for  $O$  determines the output of the model as a function of the pixel values. Thus, the causal network has depth 2, with the exogenous variables determining the feature variables, and the feature variables determining the output variable.

We also assume *causal independence* between the feature variables  $\vec{V}$ . In our setting,  $\vec{V}$  is the set of pixels of the input image, with the values capturing the color and intensity of the pixels. Pixel independence is a common assumption in explainability tools. This is a non-trivial assumption, and it might seem far-fetched, especially if we consider images capturing real objects: if a group of pixels captures, say, a cat’s ear, then a group of pixels below it should capture a cat’s eye. However, we argue that it is, in fact, accurate on images. Indeed, consider the “Photobombing” dataset, described in Section 6.1. This dataset is comprised of partially obscured images, obtained by overlaying random color patches over Imagenet images. An input from this dataset is a perfectly valid image. Indeed, obscuring a part of the input image either by introducing an artificial object or by positioning a real object in front of the primary subject of the classification does not lead to any change in unobscured pixels. For example, obscuring a cat’s ear does not lead to any change in an (unobscured) group of pixels below it, capturing a cat’s eye. Thus, pixel independence holds on general images.

We note that pixels are not concepts: a 2D image is a projection of a scene in the 3D real world on a plane; concepts that are present in the object in a real world can be invisible on this projection, hence the pixel independence.

We refer the reader to (Chockler and Halpern 2024) for a more in-depth discussion of causal independence between pixel values in image classification. We note that the causal independence assumption is not true in other types of inputs, such as tabular or spectral data. For those types of inputs, assuming independence is clearly an approximation and might lead to inaccurate results. In this paper, however, we focus on images, where causal independence between pixels holds, and it greatly simplifies explanation extraction, as we show below.

Moreover, as the causal network is of depth 2, all parents of the output variable  $O$  are contained in  $\vec{V}$ . Given these assumptions, the probability on contexts directly corresponds to the probability on seeing various images (which the model presumably learns during training).

Given an input image  $I$ , the set of contexts  $\mathcal{K}$  that we consider for an explanation is the set  $\mathcal{K}_I$  obtained by *all partial occlusions* of  $I$ , where an occlusion sets a part  $\vec{Y}$  of the image to a predefined masking color  $\vec{y}$ . The probability distribution over  $\mathcal{K}_I$  is assumed to be uniform.

Under the assumptions above, the following definition is equivalent to Definition 3.2, as shown by (Chockler and Halpern 2024).

**Definition 4.1** (Explanation for image classification). An explanation is a minimal subset of pixels of a given input image that is sufficient for the model  $\mathcal{N}$  to classify the image, where “sufficient” is defined as containing only this subset of pixels from the original image, with the other pixels set to the masking color.

As our goal is ranking of the pixels according to their importance for the classification, we only consider *singleton causes*, that is, causes consisting of one pixel and its value. Moreover, for each pixel we only consider two possible values: its original value in the image and a masking color.

**Definition 4.2** (Singleton cause for image classification). For an image  $x$  classified by the DNN as  $f(x) = o$ , a pixel  $p_i$  of  $x$  and its value in  $x$  is a *cause* of  $o$  iff there exists a subset  $P_j$  of pixels of  $x$  such that the following conditions hold:

**SC1.**  $p_i \notin P_j$ ;

**SC2.** changing the color of any subset  $P'_j \subseteq P_j$  to the masking color does not change the classification;

**SC3.** changing the color of  $P_j$  and the color of  $p_i$  to the masking color changes the classification.

We call such  $P_j$  a *witness* to the fact that  $p_i$  is a cause of  $x$  being classified as  $o$ .

Definition 4.2 is equivalent to a part of a cause according to Definition 3.1 in binary causal models with all variables being independent of each other. Moreover, under these restrictions, Definition 4.2 is equivalent to the following definition, which is the original definition of an actual cause by (Halpern and Pearl 2005c).

**Definition 4.3** (Original definition of actual cause).  $\vec{X} = \vec{x}$  is an *actual cause* of  $\varphi$  in  $(M, \vec{u})$  if the following three conditions hold:

AC1.  $(M, \vec{u}) \models (\vec{X} = \vec{x})$  and  $(M, \vec{u}) \models \varphi$ .

AC2'. There exists a partition  $(\vec{Z}, \vec{W})$  of  $\vec{V}$  with  $\vec{X} \subseteq \vec{Z}$  and some setting  $(\vec{x}', \vec{w}')$  of the variables in  $(\vec{Z}, \vec{W})$  such that if  $(M, \vec{u}) \models Z = z^*$  for  $Z \in \vec{Z}$ , then

1.  $(M, \vec{u}) \models [\vec{X} \leftarrow \vec{x}', \vec{W} \leftarrow \vec{w}'] \neg \varphi$ . In other words, changing the values of  $(\vec{X}, \vec{W})$  from  $(\vec{x}, \vec{w})$  to  $(\vec{x}', \vec{w}')$  changes  $\varphi$  from true to false;
2.  $(M, \vec{u}) \models [\vec{X} \leftarrow \vec{x}, \vec{W} \leftarrow \vec{w}', \vec{Z}' \leftarrow \vec{z}^*] \varphi$  for all subsets  $\vec{Z}'$  of  $\vec{Z}$ . In other words, setting  $\vec{W}$  to  $\vec{w}'$  should have no effect on  $\varphi$  as long as  $\vec{X}$  is kept at its current value  $\vec{x}$ , even if all the variables in an arbitrary subset of  $\vec{Z}$  are set to their original values in the context  $\vec{u}$ .

AC3.  $\vec{X}$  is minimal; there is no strict subset  $\vec{X}'$  of  $\vec{X}$  that satisfies AC1 and AC2'.

The equivalence is based on the following observations. The minimality is satisfied due to only considering singletons. The set  $\vec{Z}$  does not play a role due to the independence between the pixels. Removing  $\vec{Z}$  and the minimality condition from Definition 4.3 we get Definition 4.2.

Computing causality in image classification is, therefore, NP-complete, based on the above equivalence and the result by (Eiter and Lukasiewicz 2002), who proved NP-completeness of Definition 4.3 for binary causal models. Moreover, following the same reasoning, Definition 4.1 is equivalent to the definition of explanation by (Halpern and Pearl 2005b) for binary causal models, which is DP-complete (Eiter and Lukasiewicz 2004). Hence, there is little hope to find an efficient algorithm for computing exact explanations for image classification.

Finally, the following definition of the degree of responsibility holds for the case of image classifiers and singleton causes as in Definition 4.2.

**Definition 4.4** (Simplified responsibility). The *degree of responsibility*  $r(p_i, x, o)$  of  $p_i$  for  $x$  being classified as  $o$  is defined as  $1/(k + 1)$ , where  $k$  is the size of the smallest witness set  $P_j$  for  $p_i$ . If  $p_i$  is not a cause,  $k$  is defined as  $\infty$ , and hence  $r(p_i, x, o) = 0$ . If changing the color of  $p_i$  alone to the masking color results in a change in the classification, we have  $P_j = \emptyset$ , and hence  $r(p_i, x, o) = 1$ .

**RQ2** Can we compute explanations based on the definition above without opening the black box? What is the complexity of such computation?

The complexity of actual causality implies the intractability of the degree of responsibility of pixels in image classification as well (more precisely, computing responsibility of pixels for the classification in our setting is  $\text{FP}^{\text{NP}[\log n]}$ -complete). The following observation describes a brute-force approach to computing responsibility, which is clearly exponential in the number of pixels of the image.

**Observation 4.5.** Given an image  $x$  and its classification  $o$ , we can calculate the degree of responsibility of each pixel  $p_i$  of  $x$  by directly applying Definition 4.2, that is, by checking the conditions SC1, SC2, and SC3 for all subsets  $P_j$  of pixels of  $x$  and then choosing a smallest witness subset. While there is an underlying Boolean formula that determines the classification  $o$  given the values of the pixels of  $x$ , we do not

need to discover this formula in order to calculate the degree of responsibility of each pixel of  $x$ .

In the next section we introduce a *compositional approach* to computing approximate explanations. The main idea is first to rank pixels according to their approximate degree of responsibility, and then use a greedy approach to extract (approximate) explanations. The algorithm for computing an approximate degree of responsibility is based on the notion of a *super-pixel*  $P_i$ , which is a subset of pixels of a given image. Given an image  $x$ , we partition it into a small number of superpixels and compute their degree of responsibility for the output of the DNN. Then, we only refine those superpixels with a high responsibility (exceeding a predefined threshold). The scalability of the approach relies on the following observation, which is shown to be heuristically true in our experiments.

**Observation 4.6.** The pixels with the highest responsibility for the DNN's decision are located in super-pixels with the highest responsibility.

Intuitively, the observation holds when pixels with high responsibility do not appear in the superpixels surrounded by other pixels with very low responsibility for the input image classification outcome. While this can happen in principle, we do not encounter this case in practice owing to the continuous nature of images (even when the explanation is non-contiguous). This property is key to the success of our algorithm.

## 5 Compositional Explanations

We recall the third research question.

**RQ3** Is there an efficiently computable approximation to explanations?

We answer this question affirmatively, by presenting our *greedy compositional explanation (CE)* algorithm. The general idea is to calculate the responsibility of a superpixel and recursively distribute this responsibility to all pixels within this superpixel. The CE approach in this work consists of the following steps.

1. Given a set of superpixels, compute the responsibility of each superpixel (Section 5.1).
2. Following the responsibility result in Step 1, further refine the superpixel and calculate the responsibility for the refined superpixels (Section 5.2).

We note that the ranking depends on the selected partition. To ameliorate the effect of a particular partition, the algorithm is re-run a number of times with partitions selected independently at random, and the results are averaged across all the partitions (see Section 5.3). Section 5.4 gives a step-by-step example to illustrate the working of the algorithm.

### 5.1 Computing the responsibility of a superpixel

Given a set of pixels  $\mathcal{P}$ , we use  $\mathbb{P}_i$  to denote a *partition* of  $\mathcal{P}$ , that is, a set  $\{P_{i,j} : \bigcup P_{i,j} = \mathcal{P} \text{ and } \forall j \neq k, P_{i,j} \cap P_{i,k} = \emptyset\}$ . The number of elements in  $\mathbb{P}_i$  is a parameter, denoted by  $s$ ; in this work, we consider  $s = 4$ . We refer to  $P_{i,j}$  as

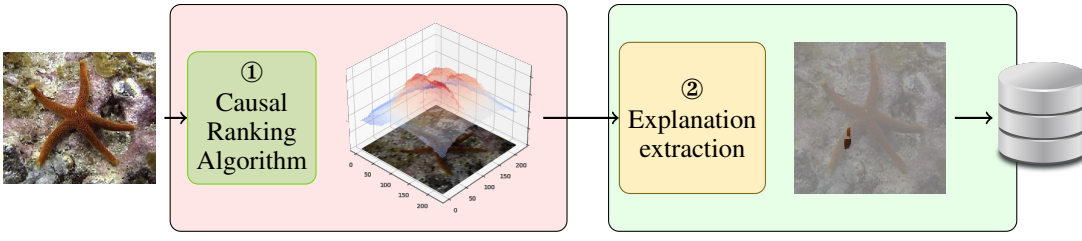


Figure 2: High level overview of Algorithm 3. Iterating parts 1 and 2 of the algorithm produce a responsibility map (①). The pixels in the image are then ordered by their approximate responsibility and used to produce a minimal sufficient explanation (②), which captures all that the DNN needs to give a classification 'starfish'.

---

**Algorithm 1** *responsibility*( $x, \mathbb{P}_i$ )

---

**INPUT:** an image  $x$ , a partition  $\mathbb{P}_i$

**OUTPUT:** a responsibility map  $\mathbb{P}_i \rightarrow \mathbb{Q}$

```

1: for each  $P_{i,j} \in \mathbb{P}_i$  do
2:    $k \leftarrow \min_{x_m} \{ \text{diff}(x_m, x) \mid x_m \in \tilde{X}_i^j \}$ 
3:    $r_{i,j} \leftarrow \frac{1}{k+1}$ 
4: end for
5: return  $r_{i,0}, \dots, r_{i,|\mathbb{P}_i|-1}$ 

```

---

*superpixels*. It is insufficient to consider each superpixel in isolation: there is no reason why anyone super pixel should be the cause of a classification. Therefore we create combinations of superpixels from the power set of  $\mathbb{P}_i$ , denoted  $2^{\mathbb{P}_i}$ .

For an NN  $\mathcal{N}$ , an input  $x$ , and a partition  $\mathbb{P}_i$ , we can generalize Def. 4.2 to the set of *superpixels* defined by  $\mathbb{P}_i$ . We denote by  $r_i(P_{i,j}, x, \mathcal{N}(x))$  the *degree of responsibility* of a superpixel  $P_{i,j}$  for  $\mathcal{N}$ 's classification of  $x$ , given  $\mathbb{P}_i$ .

For a partition  $\mathbb{P}_i$ , we denote by  $X_i$  the set of *mutant images* obtained from  $x$  by masking subsets of  $2^{\mathbb{P}_i}$ , and by  $\tilde{X}_i$  the subset of  $X_i$  that is classified as the original image  $x$ . Formally,

$$\tilde{X}_i = \{x_m : \mathcal{N}(x_m) = \mathcal{N}(x)\}.$$

We compute  $r_i(P_{i,j}, x, \mathcal{N}(x))$ , the responsibility of each superpixel  $P_{i,j}$  in the classification of  $x$ , in Algorithm 1. For a superpixel  $P_{i,j}$ , we define the set

$$\tilde{X}_i^j = \{x_m : P_{i,j} \text{ is not masked in } x_m\} \cap \tilde{X}_i.$$

For a mutant image  $x_m$ , we define  $\text{diff}_i(x_m, x)$  as the number of superpixels in the partition  $\mathbb{P}_i$  that are masked in  $x_m$  (that is, the difference between  $x$  and  $x_m$  with respect to  $\mathbb{P}_i$ ). For an image  $y$ , we denote by  $y(P_{i,j})$  an image that is obtained by masking the superpixel  $P_{i,j}$  in  $y$ . The degree of responsibility of a superpixel  $P_{i,j}$  is calculated by Algorithm 1 as a minimum difference between a mutant image and the original image over all mutant images  $x_m$  that do not mask  $P_{i,j}$ , are classified the same as the original image  $x$ , and masking  $P_{i,j}$  in  $x_m$  changes the classification.

## 5.2 Iterative refinement of responsibility

Algorithm 1 calculates the responsibility of each superpixel, subject to a given partition. Then, it proceeds with only the high-responsibility superpixels. Note that in general, it is possible that all superpixels in a given partition have the same responsibility. Consider, for example, a situation where the explanation is right in the middle of the image, and our partition divides the image into four quadrants. Each quadrant would be equally important for the classification, hence we would not gain any insight into why the image was classified in that particular way. In this case, the algorithm chooses another partition. It can also be the case that there might be multiple disjoint combinations of high responsibility superpixels in  $\mathbb{P}_i$ . Refining them all can be computationally expensive. ReX allows the user to choose from various pruning strategies to reduce the amount of work performed.

Different combinations of superpixels may have equal explanatory power. In the event that one superpixel is all that is required, therefore having responsibility 1, the further iterative subdivision of that superpixel is easy. However, if responsibility is split over multiple superpixels, we need a more refined approach. Take, for example, a situation where the right hand side of the image contains the explanation, as can be seen in Figure 6b. Here responsibility is split over two super pixels. Let us say that the passing combination of superpixels  $P_c = \{0, 2\}$ , assuming that we have numbered  $P_{i,j}$  consecutively, and that  $s = 4$ . Each superpixel  $P_{i,j}$  has responsibility 0.5. We cannot simply mask superpixel 2 while the refining superpixel 0 as both together are required for the classification. We handle this problem by holding one superpixel to its original value while refining the other and then flipping the procedure. The superpixel held to its original value, but not being refined, does not get additional responsibility. This procedure is relatively scalable to sets containing more than 2 superpixels. In our implementation, ReX,  $s$  is hard-coded to 4 because this result in powerset of superpixels of manageable size and the refinement process for sets of superpixels just discussed needs to handle at most three superpixels at a time.

One partition is rarely sufficient for a high-quality explanation, therefore we compute Algorithm 1 many times and compose the results, as shown in Algorithm 2. This calculates the responsibility for each superpixel (Line 1). If the termination condition is met (Lines 2–3), the responsibility map  $Q$  is updated accordingly. Otherwise, for each super-



---

**Algorithm 2** *iterative\_responsibility\_refinement*( $x, \mathbb{P}_i$ )

---

**INPUT:** an image  $x$  and a partition  $\mathbb{P}_i$ **OUTPUT:** a responsibility map  $\mathbb{P}_i \rightarrow \mathbb{Q}$ 

```
1:  $R \leftarrow \text{responsibility}(x, \mathbb{P}_i)$ 
2: if  $R$  meets termination condition then
3:   return  $R$ 
4: end if
5:  $R' \leftarrow \emptyset$ 
6: for each  $P_c \in (2^{\mathbb{P}_i} - \emptyset)$  s.t.  $R(P_c) \neq 0$  do
7:    $R' \leftarrow R' \cup \text{iterative\_responsibility\_refinement}(x, P_c)$ 
8: end for
9: return  $R'$ 
```

---

pixel in  $\mathbb{P}_i$ , we refine it and call the algorithm recursively. We use  $\cup$  to include these newly computed values in the returned map. The algorithm terminates when: 1) the superpixels in  $\mathbb{P}_i$  are sufficiently refined (containing only very few pixels), or 2) when all superpixels in  $\mathbb{P}_i$  have the same responsibility (this condition is for efficiency).

### 5.3 Explanation extraction

So far, we assume one particular partition  $\mathbb{P}_i$ , which Algorithm 2 recursively refines and calculates the corresponding responsibilities of superpixels in each step by calling Algorithm 1. We note that the choice of the initial partition over the image can affect the values calculated by Algorithm 2, as this partition determines the set of possible mutants in Algorithm 1. We ameliorate the influence of the choice of any particular partition by iterating the algorithm over a set of partitions. Twenty iterations of the algorithm will therefore yield 20 starting partitions, chosen at random. ReX allows the user to choose from a number of different types of random to build these partitions, with uniform being the default.

In Algorithm 3, we consider  $N$  initial partitions and compute an average of the degrees of responsibility induced by each of these partitions. In the algorithm,  $\mathbb{P}^x$  stands for a specific partition chosen randomly from the set of partitions, and  $r_p$  denotes the degree of responsibility of a pixel  $p$  w.r.t.  $\mathbb{P}^x$ .

Algorithm 3 has two parts: ranking all pixels (Lines 1–9) and constructing the explanation (Lines 10–17). The algorithm ranks the pixels of the image according to their responsibility for the model’s output. Each time a partition is randomly selected (Line 3), the iterative responsibility refinement (Algorithm 2) is called to refine it into a set of fine-grained superpixels and calculate their responsibilities (Line 4). A superpixel’s responsibility is evenly distributed to all its pixels, and the pixel-level responsibility is updated accordingly for each sampled partition (Lines 5–7). After  $N$  iterations, all pixels are ranked according to their responsibility  $r_p$ .

The remainder of Algorithm 3 follows the method for explaining the result of an image classifier by (Sun et al. 2020). That is, we construct a subset of pixels  $\mathcal{E}$  to explain  $\mathcal{N}$ ’s output on this particular input  $x$  greedily. We add pixels to  $\mathcal{E}$  as long as  $\mathcal{N}$ ’s output on  $\mathcal{E}$  does not match  $\mathcal{N}(x)$ . This process

---

**Algorithm 3** *explanation*( $x$ )

---

**INPUT:** an input image  $x$ , a parameter  $N \in \mathbb{N}$ **OUTPUT:** an explanation  $\mathcal{E}$ 

```
1:  $r_p \leftarrow 0$  for all pixels  $p$ 
2: for  $c$  in 1 to  $N$  do
3:    $\mathbb{P}^x \leftarrow \text{sample a partition}$ 
4:    $R \leftarrow \text{iterative\_responsibility\_refinement}(x, \mathbb{P}^x)$ 
5:   for each  $P_{i,j} \in \text{domain of } R$  do
6:      $\forall p \in P_{i,j} : r_p \leftarrow r_p + \frac{R(P_{i,j})}{|P_{i,j}|}$ 
7:   end for
8: end for
9:  $\text{pixel\_ranking} \leftarrow \text{pixels from high } r_p \text{ to low}$ 
10:  $\mathcal{E} \leftarrow \emptyset$ 
11: for each pixel  $p_i \in \text{pixel\_ranking}$  do
12:    $\mathcal{E} \leftarrow \mathcal{E} \cup \{p_i\}$ 
13:    $x^{exp} \leftarrow \text{mask pixels of } x \text{ that are not in } \mathcal{E}$ 
14:   if  $\mathcal{N}(x^{exp}) = \mathcal{N}(x)$  then
15:     return  $\mathcal{E}$ 
16:   end if
17: end for
```

---

terminates when  $\mathcal{N}$ ’s output is the same as on the whole image  $x$ . The set  $\mathcal{E}$  is returned as an explanation. We note that this extraction procedure is not normally followed by other familiar XAI tools, as their several different definitions of explanation do not extend to finding minimal sets of pixels which induce the desired classification.

While we approximate the computation of an explanation in order to ensure efficiency of our approach, the algorithm is built on solid theoretical foundations, which distinguishes it from other random or heuristic-based approaches. In practice, while our algorithm uses an iterative average of a greedy approximation, it yields highly accurate results (Section 6). Furthermore, our approach is simple and general, and uses the neural network as a blackbox.

### 5.4 Illustrative example

To illustrate how ReX works, consider Figure 3, which is classified as ‘bus’ by ResNet50, even though there is an occlusion in the middle. Initially, ReX picks up an arbitrary partition of the image with four superpixels. This results in 15 combinations of masking superpixels, though in practice, we only need to examine 14 combinations as the 15<sup>th</sup> is the entire image, which we have already tested. We use Algorithm 1 to calculate the responsibility of each superpixel. Those superpixels or combinations of superpixels which contribute towards the correct classification of further refined. This iterative refinement is a recursive application of the same initial random partitioning into four superpixels, as in Algorithm 2.

The responsibility mapss shown in Figure 4 demonstrate the importance of Algorithm 3. The initial partitioning of the image can greatly affect the quality of the responsibility map. Figure 4a shows the responsibility map after one iteration of the algorithm. While it still indicates well the areas of interest in the image it is also quite rectilinear. Fig-

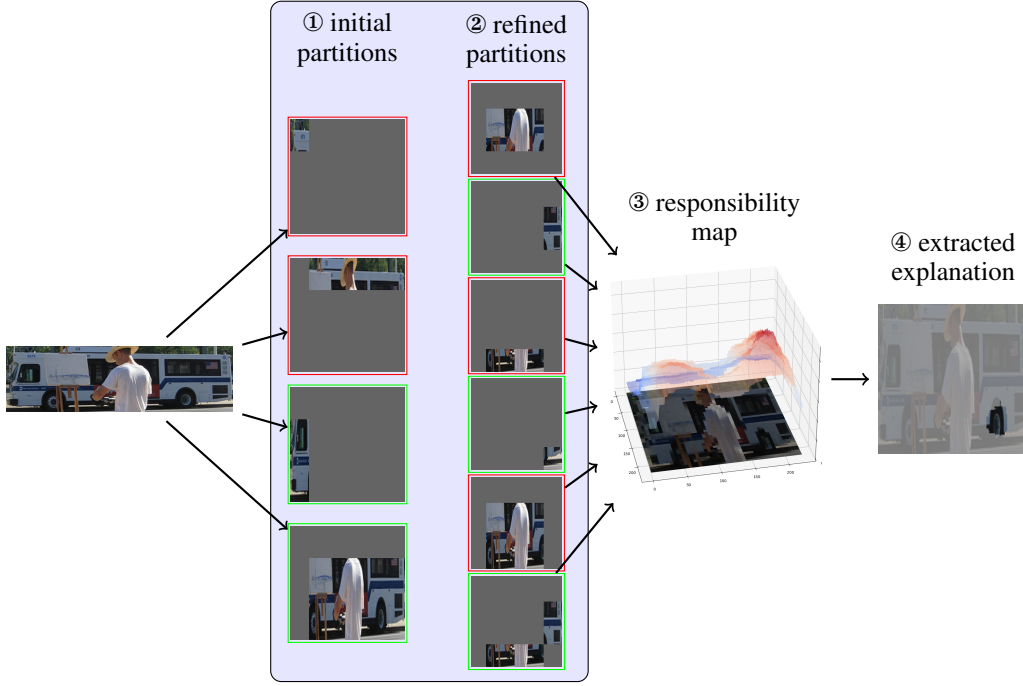


Figure 3: The ReX algorithm in action: ReX creates an initial random partition of an image into 4 sections (①). All combinations of these sections are queried by the model, with further random refinement applied to those sections or combinations of sections that meet the requirements (②). Some combinations, highlighted in green, are classified as bus, others, in red, are not. This results, after several iterations, in a detailed responsibility map (③), from which a minimal passing explanations can be extracted (④).

ure 4b contains a lot more information about the distribution of responsibility over the pixels in the image. We now have two distinct peaks of responsibility on either side of the central occlusion (a person). Further iterations cause further refinement. By iteration 100 (Figure 4e), it is clear that the dominant explanation is around the rear tyre of the bus. The other explanation however, while depressed in relation to the tyre, has not vanished and can still be found through searching the responsibility map (Chockler, Kelly, and Kroening 2023). Indeed, a disjoint explanation exists for this image, as given in Figure 5a.

### 5.5 Termination and complexity

It is clear that the algorithm terminates as soon as the parts can no longer be divided into superpixels. Moreover, the number of calls it performs to the model is linear in the size of the image, as proved in the following lemma.

**Lemma 5.1.** *The number of calls of Algorithm 3 to the model is  $O(2^s n N)$ , where  $s$  is the size of the partition in each step (in our setting  $s = 4$ ),  $n$  is the number of pixels in the original image  $x$ , and  $N$  is the number of initial partitions.*

*Proof.* The computation of responsibilities of superpixels in one partition is  $O(2^s)$ , as the algorithm examines the effect of mutating each subset of the superpixels in the current partition. Note that  $s$  is a constant independent of the size of

the image. The number of steps is determined by the termination condition on the size of a single superpixel, which in the worst case is the same as a single pixel. In our setting, the algorithm terminates when a single superpixel is smaller contains fewer than 10 pixels<sup>1</sup>. However, in general, the algorithm can continue down to the level of a single pixel, thus resulting in  $n$  pixels in the last step. The algorithm performs  $N$  iterations, and every iteration uses a different initial partition. The parameter  $N$  is independent of the size of the image.  $\square$

## 6 Evaluation

We conduct a large scale investigation into ReX, comparing it with a host of popular XAI tools. Our answers to the research questions will largely remain empirical. Just as there is no universally agreed definition of explanation, there is also no single best way to evaluate the quality of an explanation.

**RQ4** What are suitable quality measures for explanations?

A measure is suitable if it is meaningful with respect to quality and produces results that match our intuition.

A causal explanation is a minimal set of pixels from an image which are sufficient to obtain the same top classification.

<sup>1</sup>ReX also terminates when no combination of active superpixels has the required classification or a user-defined work budget is exceeded.



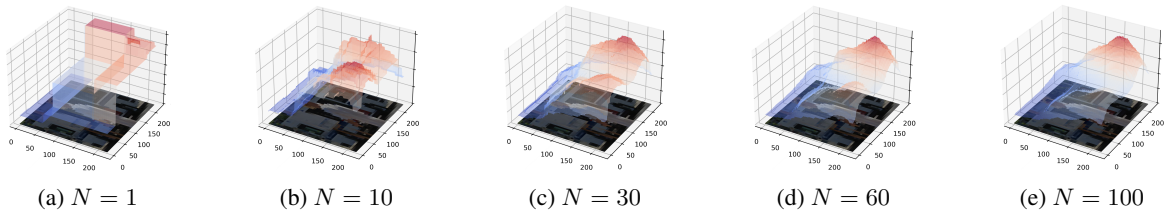


Figure 4: Improvement of ReX’s pixel ranking as the number of iterations  $N$  increases (Algorithm 3)



(a) Non-contiguous explanation



(b) Contiguous explanation

Figure 5: Two different explanations extracted from the 30 iteration ranking in Figure 4. Figure 5a contrasts interestingly with Figure 5b: it seems that the front tire by itself is not sufficient (a very small rectangular section of the rear tire is included in the explanation), but the rear tire is.

cation as the complete set of all pixels of an image. This immediately suggests size of explanation as a robust quality measure. As none of the tools (apart from ReX) compute minimal, sufficient explanations, we use the mechanism of extraction (Section 5.3) on the output of all tools tested. We also use the same approach to compute insertion and deletion curves over all XAI outputs.

**Utility and interpretation of deletion curves** When insertion and deletion curves were introduced in RISE (Petsiuk, Das, and Saenko 2018), the authors stated that a high insertion and a low deletion is preferable. This assertion relies on the assumption that there is only one explanation for the image’s classification, or that the XAI tool finds only one explanation. Moreover, saliency values outside of the single ‘explanation’ must be strictly uninformative: in order to keep deletion low, the saliency map cannot provide information about any substructures present in the image. Pixels must be added back into the image in an order that is essentially random. ReX does not work like this: the responsibility map provides detail over the entire pixel space.

As an example, if we examine Figure 6a, we have an image with a normalized insertion curve of 0.97 but a normalized deletion curve of 0.32. There would appear to be tension between the two numbers, as a high insertion suggests a high quality explanation whereas a high deletion suggests a low quality explanation. The mystery is resolved, however, by noting that images can and do contain multiple explanations, as first shown in (Shitole et al. 2021). Indeed, there are four distinct peaks of responsibility in Figure 6a, each of which corresponds to an independent explanation for starfish (Figure 7).

The deletion score is high because the responsibility map is informative even for the more lowly ranked pixels. In the multiple explanation scenario, one would expect a high deletion score. Uniquely among the tools examined

here, ReX supports multiple explanations for an image natively (Chockler, Kelly, and Kroening 2023). In Tables 1 to 3 we follow the usual procedure of indicating the lowest deletion curve value, but stress that lowest does not necessarily indicate best.

We quantify the quality of the explanations with several complementary methods. First, we calculate the minimal explanation size as a percentage of the size of the image. This coincides with Definition 3.2. It also gives an idea of how concentrated the responsibility or saliency maps provided by the XAI tools are. The smaller the area of the explanation, the more the XAI tool was able to isolate precisely those pixels (and only those pixels) required to match the original classification.

Furthermore, we calculate *normalized* insertion and deletion curves for all images. As stated above, it is not clear how to compare the area under curve (AUC) of a low confidence image against a high confidence image to derive an average AUC performance. It is, after all, not the fault of the XAI tool that the confidence of the model is low on any particular image. To overcome this problem, we follow (Calderón-Peña, Chockler, and Kelly 2024) and normalize all curves by the initial confidence of the model on image under test. Note that this can result in the the insertion curve AUC being greater than 1. This phenomenon occurs when the confidence on the overall image is lower than the confidence of intermediate insertion stages. This makes intuitive sense: if the pixel ranking is accurate, then those pixels that either do not contribute towards the classification, or reduce confidence, are left to be added last. Without these pixels, confidence is potentially much higher.

**Comparison with human segmentation** For those datasets that contain segmentation information, we also measure the intersection of the minimal explanation with the segmentation. This segmentation is human-provided

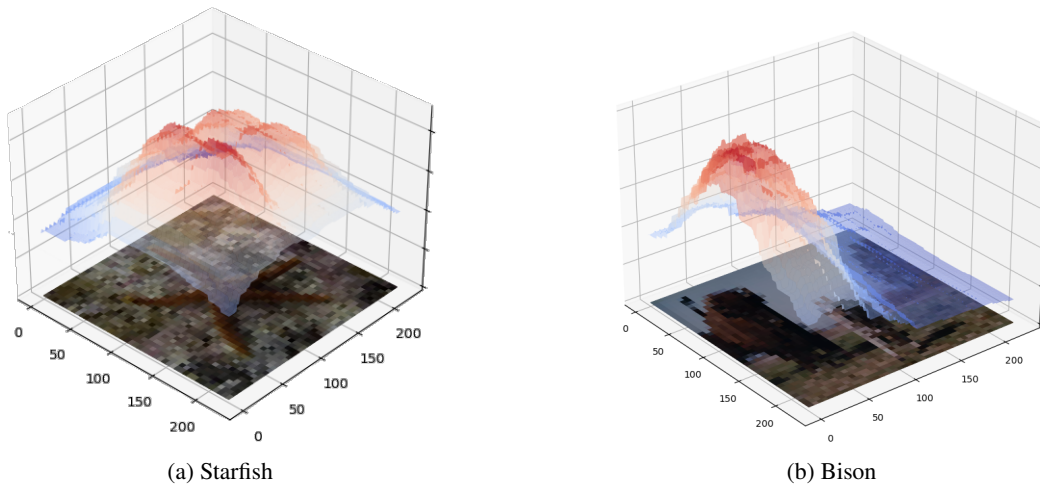


Figure 6: An image with a high deletion curves does not indicate a low quality explanation. The starfish (Figure 6a) has a normalized deletion of 0.32 because there are multiple points of high responsibility in the image. These points indicate the presence of multiple explanations. The bison (Figure 6b) has a low deletion of 0.1 because there is only one point of interest in the image. Deletion is a difficult measure to interpret.

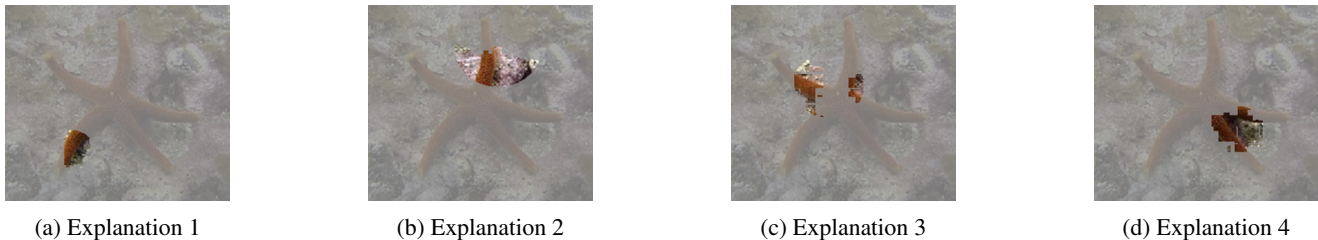


Figure 7: The responsibility map ReX provides is sufficiently detailed to extract multiple valid explanations for most images. These starfish explanations were extracted from Figure 6a).

and we argue corresponds most closely with what a human considers acceptable. On VOC2012, for example, we would like an minimal explanation to reside mostly inside the human-provided segmentation mask and therefore contain only a small number of pixels outside the mask. For datasets that feature occluded objects, a good explanation would have as few pixels from inside the occlusion as possible, as the occlusion should not make a contribution towards the model’s classification.

To answer **RQ4**, we argue that the size of explanations, as well as insertion curves and the intersection with the occlusion are measures that match our intuition. However, we argue that deletion curves are not, as they remain high in presence of multiple explanations.

## 6.1 Experimental Setup

We answer research questions **RQ5–RQ7** experimentally. We have implemented the proposed explanation approach in the publicly available tool ReX. For all other XAI tools, apart from RISE, we used the Captum PyTorch library (Kokhlikyan et al. 2020)<sup>2</sup>. For RISE, we used the au-

thors’ implementation<sup>3</sup>, which we lightly altered to use PyTorch rather than tensorflow.

In the evaluation, we compare ReX with a wide range of explanation tools, specifically GRAD-CAM (Selvaraju et al. 2017), KERNELSHAP (Lundberg and Lee 2017a), GRADIENTSHAP (Lundberg and Lee 2017b), RISE (Pet-siuk, Das, and Saenko 2018), LIME (Ribeiro, Singh, and Guestrin 2016), IG (Sundararajan, Taly, and Yan 2017), NoiseTunnel (Smilkov et al. 2017). For the ResNet50 model only, we also include LRP. We were unable to make the captum version of LRP run on either the ViT or the ConvNext model.

While our main interest is in black-box explainability, we have included methods which require access to the model gradient, such as GradientsHAP and IG, and internal model layers, *i.e.* GRAD-CAM. We call those tools which require internal access to the model ‘white-box’; those that require the access to the gradient we term ‘grey-box’, and those that just need the model’s classification, we call ‘black-box’. ReX is a black-box method. PyTorch permits optional access to the gradient, so tools such as IG require at least some flexibility when calling the model. This is not guaranteed with

<sup>2</sup><https://www.captum.ai>

<sup>3</sup><https://github.com/eclique/RISE>

proprietary models: hence our grey-box category.

We use 4 data sets: ImageNet-1k-mini validation (Rusakovsky et al. 2015), ECSSD (Shi et al. 2016), Pascal VOC2012 (Everingham et al. ), and a “Photobombing” dataset we created. Imagenet1k-mini comes with labels for ground truth. VOC2012 has labels and segmentation data. ECSSD comprises complex images which come with a human-provided segmentation. We created the “Photobombing” dataset by inserting black occlusions into ImageNet images, meaning we have the original label and also know the pixel coordinates of the occlusions. These occlusions are placed so as not to change the model classification. We use the TORCHVISION<sup>4</sup> implementations of ResNet50, ViT and ConvNext-Large with default weights on all data sets.

All experiments were conducted using a server running Ubuntu 20.04 with an Nvidia A40 GPU. Moreover, all tools were used with default settings. For ReX in particular, this means that it performs 20 iterations of the algorithm ( $N$  in Algorithm 3), with a minimum superpixel size of 10 pixels. The pruning strategy for the work queue is “area” (the passing mutants are ordered by size) and only one item is kept in the work queue at a time, so we only refine the smallest passing mutant. Partitions are created uniformly at random. Other strategies and partitioning distributions are available in the configuration.

ReX uses four superpixels per partition. This is practical for images as we can split the image with just one call to a random number generator. The number of mutants produced is also relatively small (15), which can usually be fit into a single batch for model processing. Having more initial superpixels does not lead to greater expressivity: we iteratively refine passing combinations of superpixels further, essentially recreating a more detailed initial partition produced by a greater number of superpixels. The termination conditions for the partition refinement in Algorithm 2 are: 1) the area of a superpixel is less than 10 pixels of (resized) input image, 2) the four superpixels share the same responsibility or 3) no combination of superpixels produces the desired classification.

## 6.2 Results

**RQ5** What is the precision of explanations computed by our algorithm compared to other XAI methods?

**RQ6** Is there a trade-off between precision and compute cost of the explanations?

**RQ7** Can black-box methods achieve the same quality of explanations as white and grey-box methods?

Tables 1 to 3 show the experimental results of evaluation of ReX against 8 other XAI tools over 4 datasets, with three different models. The columns in the tables are: mean area (area),  $\sigma$  of area (standard deviation), normalized insertion curves AUC (ins), normalized deletion curves AUC (del), proportion of explanation inside the relevant segment (IN), and the fraction of the explanation that is outside the relevant

segment (OUT), shown only where appropriate. Bold indicates best result in category for all columns. Note that while we have indicated lowest AUC for deletion, lower here is not necessarily better, as we argued earlier.

**Resnet** Table 1 shows the results with the ResNet50 model. ReX consistently produces the most precise explanations. This is reinforced by the observations that ReX also produces the highest insertion AUC of any of the tools. ReX does particularly well on the ‘Photobombing’ dataset, where its explanations are almost entirely (0.97) disjoint with the inserted occlusion (Figure 12). Figure 8 shows that ReX has the most concentrated explanations and consistent results, with very few outliers. The grey-box tools perform worse than the other methods. Note that ReX even outperforms GRAD-CAM.

**ViT** Table 2 shows the results with the ‘vit\_b\_32’ model from TORCHVISION. Explanations across all tools are much larger than for ResNet50model, which seems to be a feature of the model. ReX, however, still manages to produce explanations with the lowest number of redundant pixels. In general, ReX, LIME and GRAD-CAM are the best performing tools. Even in cases where LIME slightly outperforms ReX (e.g., on ECSSD IN), with 0.73 of its explanation inside the segmentation against 0.72, the effect is very small. Figure 9 shows that ReX again has the most concentrated explanations and consistent results, with very few outliers. LIME is the closest comparable tool, though it has many more outliers and a higher median value. The significant difference in explanation size between the ResNet model and ViT model is, perhaps, of independent interest.

**ConvNext** Table 3 shows the results with the ‘convnext\_large’ model from TORCHVISION. ReX, LIME, GRAD-CAM and RISE are the best performing tools. It is interesting to note that 3 of these tools fall into our ‘black-box’ category. Figure 10 shows that ReX has the best performance again, this time slightly ahead of GRAD-CAM, as GRAD-CAM has many more outliers than ReX and a slightly larger inter-quartile range. Explanation size is comparable with that of the ResNet model, making the ViT model somewhat of an outlier.

**Runtime** We measured the running time of all tools. As all tools were evaluated on the same hardware with the same models and datasets, the results should be consistent. The white and gray-box methods are clearly the fastest, as expected. Indeed, GRAD-CAM is essentially instantaneous, as the overhead over one call to the model is insignificant. No black-box tool can compete with this, by the nature of black-box tools. All the gradient based methods took  $\approx 3$  seconds to produce initial maps. While they are still fast, the quality of their explanations is lower.

Both ReX and LIME took  $\approx 4$ s to produce maps, with RISE being much slower ( $\approx 10$ s). If we take into account the extra time for the explanation extraction (which only ReX does by default), the efficiency picture changes slightly. ReX’s total

<sup>4</sup><https://pytorch.org/vision/stable/index.html>

Table 1: Results for ResNet50 model.

(a) Results on Voc

tool	area ( $\downarrow$ )	std	ins ( $\uparrow$ )	del	IN ( $\uparrow$ )	OUT ( $\uparrow$ )
GRAD-CAM	0.0832	0.1202	1.0488	0.2756	0.3202	—
NoiseTunnel	0.2867	0.2627	0.6953	0.0851	0.3241	—
LRP	0.3936	0.2828	0.5267	0.2953	0.2093	—
IG	0.4904	0.2768	0.4899	0.1228	0.2215	—
GRADIENTSHAP	0.3894	0.3002	0.5935	<b>0.0651</b>	0.2872	—
KERNELSHAP	0.7741	0.2084	0.188	0.1941	0.1636	—
LIME	0.1124	0.1616	0.963	0.2329	0.3039	—
ReX	<b>0.0427</b>	<b>0.0505</b>	<b>1.2218</b>	0.2148	<b>0.6432</b>	—
RISE	0.1271	0.1547	0.9358	0.2264	0.2861	—

(b) Results on Imagenet

tool	area ( $\downarrow$ )	std	ins ( $\uparrow$ )	del	IN ( $\uparrow$ )	OUT ( $\uparrow$ )
GRAD-CAM	0.0486	0.0839	1.0059	0.4073	—	—
NoiseTunnel	0.1847	0.2131	0.7612	0.1274	—	—
LRP	0.2749	0.2418	0.5972	0.3567	—	—
IG	0.4063	0.264	0.534	0.1767	—	—
GRADIENTSHAP	0.2861	0.2696	0.6474	<b>0.0983</b>	—	—
KERNELSHAP	0.6686	0.2472	0.2549	0.2649	—	—
LIME	0.0649	0.0969	0.9871	0.3313	—	—
ReX	<b>0.0333</b>	<b>0.0351</b>	<b>1.1101</b>	0.3403	—	—
RISE	0.1026	0.1254	0.8898	0.3728	—	—

(c) Results on “Photobombing”

tool	area ( $\downarrow$ )	std	ins ( $\uparrow$ )	del	IN ( $\uparrow$ )	OUT ( $\uparrow$ )
GRAD-CAM	0.0455	0.0642	0.9843	0.3625	—	0.8505
NoiseTunnel	0.1565	0.1832	0.7604	0.1348	—	0.8732
LRP	0.2429	0.205	0.6049	0.3687	—	0.9058
IG	0.4184	0.2311	0.5178	0.1853	—	0.8806
GRADIENTSHAP	0.296	0.2373	0.637	<b>0.114</b>	—	0.8533
KERNELSHAP	0.6601	0.2246	0.2527	0.2612	—	0.9188
LIME	0.0507	0.0523	0.9937	0.3046	—	0.8921
ReX	<b>0.0297</b>	<b>0.026</b>	<b>1.0481</b>	0.2947	—	<b>0.9739</b>
RISE	0.0787	0.0942	0.8906	0.2977	—	0.8798

(d) Results on ECSSD

tool	area ( $\downarrow$ )	std	ins ( $\uparrow$ )	del	IN ( $\uparrow$ )	OUT ( $\uparrow$ )
GRAD-CAM	0.0836	0.1288	1.0226	0.2915	<b>0.6654</b>	—
NoiseTunnel	0.2695	0.276	0.7194	0.119	0.5955	—
LRP	0.3545	0.292	0.5721	0.305	0.3418	—
IG	0.4437	0.3016	0.5552	0.1377	0.4187	—
GRADIENTSHAP	0.3525	0.3182	0.6444	<b>0.0977</b>	0.5379	—
KERNELSHAP	0.7257	0.2403	0.2348	0.2369	0.244	—
LIME	0.1013	0.1579	1.0024	0.2404	0.6538	—
ReX	<b>0.0423</b>	<b>0.0522</b>	<b>1.2176</b>	0.2214	0.6205	—
RISE	0.1165	0.1599	0.95	0.2752	0.5451	—

Table 2: Results for ViT model.

(a) Results on Voc

tool	area ( $\downarrow$ )	std	ins ( $\uparrow$ )	del	IN ( $\uparrow$ )	OUT ( $\uparrow$ )
GRAD-CAM	0.7148	0.181	0.2466	0.1889	0.1727	—
NoiseTunnel	0.4988	0.3019	0.4565	0.0633	0.2315	—
IG	0.5652	0.2632	0.4274	0.0943	0.1946	—
GRADIENTSHAP	0.5021	0.2992	0.4761	<b>0.0551</b>	0.2267	—
KERNELSHAP	0.669	0.2603	0.2579	0.2579	0.1686	—
LIME	0.277	0.2218	<b>0.7191</b>	0.112	0.26	—
ReX	<b>0.2206</b>	<b>0.1711</b>	0.6985	0.1377	<b>0.5496</b>	—
RISE	0.4049	0.2491	0.5986	0.097	0.2365	—

(b) Results on Imagenet

tool	area ( $\downarrow$ )	std	ins ( $\uparrow$ )	del	IN ( $\uparrow$ )	OUT ( $\uparrow$ )
GRAD-CAM	0.6277	0.203	0.2943	0.2538	—	—
NoiseTunnel	0.3903	0.2711	0.5341	<b>0.098</b>	—	—
IG	0.4706	0.2505	0.4833	0.1481	—	—
GRADIENTSHAP	0.3871	0.2691	0.5586	0.0916	—	—
KERNELSHAP	0.5483	0.2651	0.3541	0.3519	—	—
LIME	0.2246	0.1937	<b>0.7264</b>	0.1668	—	—
ReX	<b>0.1689</b>	<b>0.133</b>	0.687	0.2015	—	—
RISE	0.3356	0.2333	0.5997	0.1664	—	—

(c) Results on “Photobombing”

tool	area ( $\downarrow$ )	std	ins ( $\uparrow$ )	del	IN ( $\uparrow$ )	OUT ( $\uparrow$ )
GRAD-CAM	0.6025	0.1907	0.303	0.2715	—	0.9196
NoiseTunnel	0.3647	0.2447	0.5439	0.1012	—	0.8835
IG	0.4598	0.2251	0.4806	0.1486	—	0.8889
GRADIENTSHAP	0.3726	0.2465	0.5607	<b>0.0967</b>	—	0.8802
KERNELSHAP	0.5168	0.233	0.37	0.3665	—	0.9186
LIME	0.1748	0.1458	<b>0.7365</b>	0.1778	—	0.8891
ReX	<b>0.1402</b>	<b>0.1046</b>	0.6883	0.2073	—	<b>0.9551</b>
RISE	0.2803	0.2056	0.6119	0.1741	—	0.8915

(d) Results on ECSSD

tool	area ( $\downarrow$ )	std	ins ( $\uparrow$ )	del	IN ( $\uparrow$ )	OUT ( $\uparrow$ )
GRAD-CAM	0.6741	0.2181	0.2731	0.2344	0.2494	—
NoiseTunnel	0.4298	0.3001	0.5371	0.0731	0.4296	—
IG	0.4727	0.2723	0.5184	0.1082	0.3409	—
GRADIENTSHAP	0.4179	0.2929	0.5772	<b>0.0685</b>	0.4134	—
KERNELSHAP	0.6192	0.2729	0.321	0.3188	0.2466	—
LIME	0.2698	0.2319	<b>0.7392</b>	0.123	<b>0.5548</b>	—
ReX	<b>0.2008</b>	<b>0.1653</b>	0.7286	0.1475	0.5334	—
RISE	0.3687	0.2585	0.6597	0.1178	0.4468	—

Table 3: Results for convnext model.

(a) Results on Voc

tool	area ( $\downarrow$ )	std	ins ( $\uparrow$ )	del	IN ( $\uparrow$ )	OUT ( $\uparrow$ )
GRAD-CAM	0.0556	0.0948	0.8635	0.2497	0.3345	—
NoiseTunnel	0.1972	0.2443	0.689	0.117	0.3614	—
IG	0.4152	0.2565	0.465	0.2387	0.2025	—
GRADIENTSHAP	0.2268	0.2609	0.6411	<b>0.0998</b>	0.3327	—
KERNELSHAP	0.5739	0.3001	0.2926	0.2924	0.1678	—
LIME	0.0689	0.0972	0.8096	0.2908	0.3042	—
ReX	<b>0.0361</b>	<b>0.038</b>	<b>0.876</b>	0.2057	<b>0.6295</b>	—
RISE	0.0759	0.1129	0.8136	0.3005	0.2863	—

(b) Results on Imagenet

tool	area ( $\downarrow$ )	std	ins ( $\uparrow$ )	del	IN ( $\uparrow$ )	OUT ( $\uparrow$ )
GRAD-CAM	0.0337	0.0553	0.8613	0.4413	—	—
NoiseTunnel	0.1116	0.1608	0.7682	<b>0.1886</b>	—	—
IG	0.3414	0.2168	0.4993	0.3471	—	—
GRADIENTSHAP	0.1394	0.183	0.706	0.1678	—	—
KERNELSHAP	0.4357	0.2855	0.4042	0.4061	—	—
LIME	0.0493	0.0707	0.8228	0.4747	—	—
ReX	<b>0.0287</b>	<b>0.0236</b>	<b>0.8788</b>	0.3487	—	—
RISE	0.0615	0.084	0.8058	0.5136	—	—

(c) Results on “Photobombing”

tool	area ( $\downarrow$ )	std	ins ( $\uparrow$ )	del	IN ( $\uparrow$ )	OUT ( $\uparrow$ )
GRAD-CAM	0.0426	0.0527	0.8584	0.3688	—	0.8695
NoiseTunnel	0.0768	0.0925	0.7916	<b>0.2077</b>	—	0.8755
IG	0.3144	0.1731	0.5454	0.3847	—	0.8783
GRADIENTSHAP	0.1335	0.1351	0.7095	0.2186	—	0.85
KERNELSHAP	0.3829	0.2405	0.4683	0.468	—	0.9183
LIME	0.0513	0.0551	<b>0.8643</b>	0.4161	—	0.8947
ReX	<b>0.0296</b>	<b>0.0236</b>	0.8475	0.3173	—	<b>0.9748</b>
RISE	0.063	0.0723	0.8129	0.4769	—	0.9015

(d) Results on ECSSD

tool	area ( $\downarrow$ )	std	ins ( $\uparrow$ )	del	IN ( $\uparrow$ )	OUT ( $\uparrow$ )
GRAD-CAM	0.0574	0.1023	0.8865	0.2694	<b>0.6846</b>	—
NoiseTunnel	0.2164	0.2734	0.6424	0.1067	0.5913	—
IG	0.421	0.2925	0.4202	0.2102	0.363	—
GRADIENTSHAP	0.2434	0.284	0.5911	<b>0.0987</b>	0.5671	—
KERNELSHAP	0.5616	0.3152	0.2898	0.2977	0.2468	—
LIME	0.0849	0.1377	0.7157	0.3183	0.5841	—
ReX	<b>0.0364</b>	<b>0.0405</b>	<b>0.9012</b>	0.2077	0.5722	—
RISE	0.0823	0.1387	0.7996	0.3073	0.5045	—



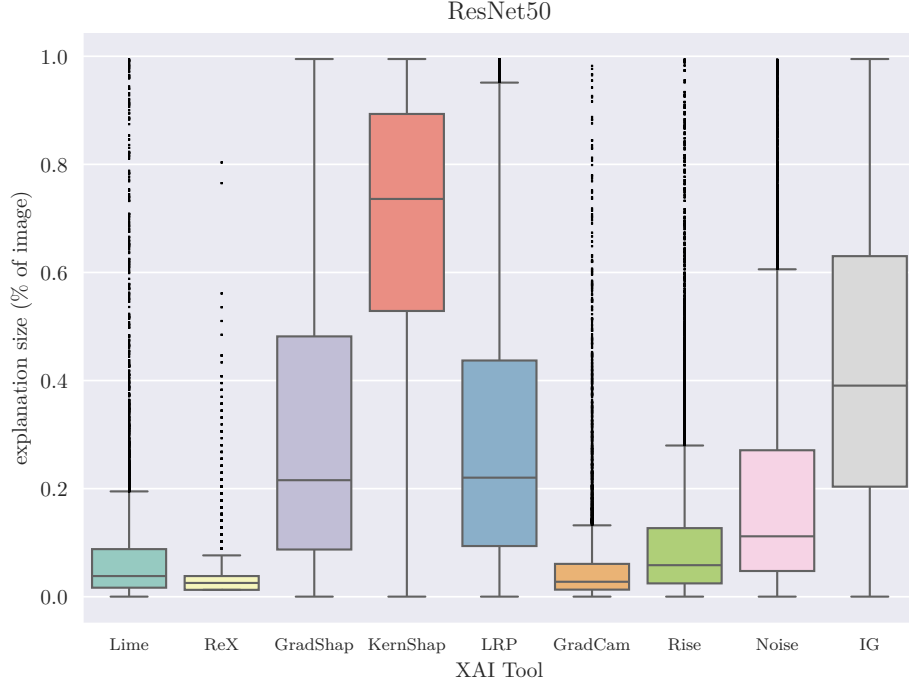


Figure 8: Box plot of all tools over all datasets with a ResNet50 model. ReX has the lowest median value and also the smallest number of outliers.

compute time increases only slightly (to  $\approx 6$ s) due to the uniformly small size of its explanations. Other tools suffer more though, even GRAD-CAM’s average compute time increases to  $\approx 4$ s. ReX is an efficient black-box tool: for **RQ6** therefore, our results show that there is little trade-off between quality and compute cost.

### 6.3 Discussion

Broadly speaking, the tools can be split into three different sets. The gradient-based methods perform least well on all metrics, including overlap with a human-provided segmentation mask. The explanations they provide are diffuse and large. NoiseTunnel uses IG as its primary saliency method, and in return for a relatively small computational overhead, NoiseTunnel greatly improves the explanation quality over the IG baseline.

Figure 11 shows cumulative plots of explanation sizes over the different tested models. Again, ReX dominates the other curves. LIME and GRAD-CAM are, in general, the next best performing tools. The poor performance (almost linear) of KERNELSHAP is interesting, suggesting that image explainability is not a natural fit for this method.

LIME, when used for image classification, works best when provided with a segmentation mask of the image. For common datasets such as the ones we investigate, many high quality algorithms exist. ReX does not require such existing segmentation masks. (Blake et al. 2023) conducted an investigation on brain MRI explainability using a different model

and different data set and a similar, though not overlapping, set of explainability tools. On this dataset, LIME’s performance is hampered by medically meaningless segmentation. They found that ReX did not suffer from this problem, but performed well compared to the other tools on this different model and data.

The performance of ReX is notable across all datasets for being very consistent in terms of the evaluation metrics. The other tools examined are not as consistent. Note that the values for IN and OUT in Tables 1 to 3 are percentages of the explanation contained (or outside) the segmentation. As ReX’s explanations are already smaller than the others, this means that, in absolute terms, ReX also has fewer extraneous pixels. This holds because other tools (such as LIME) may have similar IN values, but a larger explanation size.

We evaluated the results produced by ReX with those produced by other explainability tools on a number of standard measures proposed in the literature, such as the size of explanations, insertion and deletion curves. For the datasets containing the ground truth or some part of it, such as the segmentation information or the partial occlusion, we also measured the percentage of the explanation that is clearly outside of an area where it should be contained (such as the occlusion in partially occluded areas). For all other measures, ReX shows superior performance, which answers **RQ5**.

Finally, for **RQ7**, we did not exhaustively compare the results against all possible explainability methods. Rather, we chose the state-of-the-art primary attribution methods from

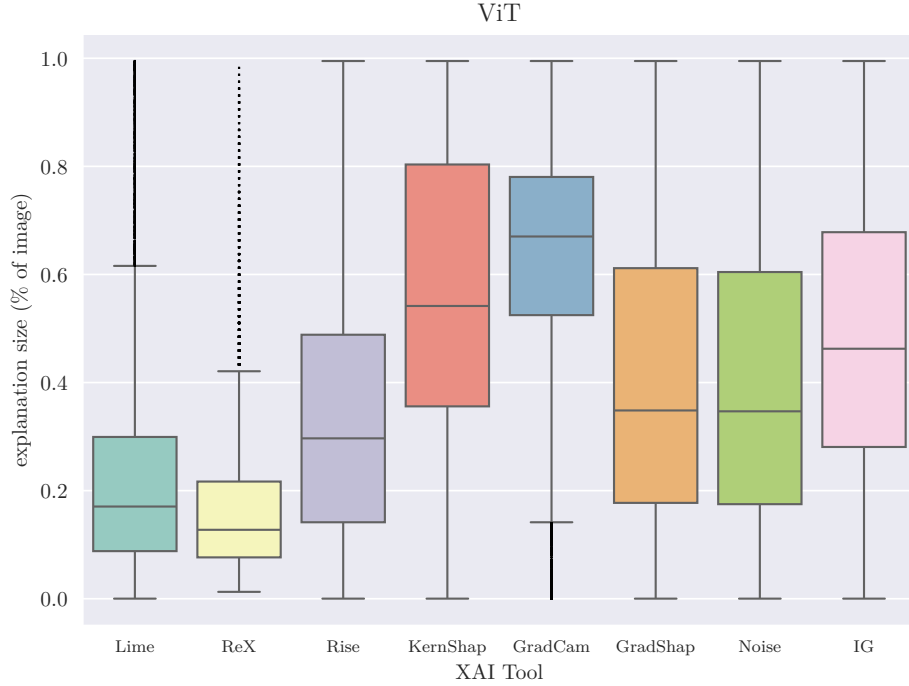


Figure 9: Box plot of all tools over all datasets with a ViT model. ReX has the lowest median value and also the smallest number of outliers. ViT explanations are noticeably larger than those for ResNet50 and ConvNext.

the Captum library.

## 7 Conclusions and Future Work

In this paper we described an approach to explainability of image classifiers that is rooted in actual causality and computes explanations based on the formal definitions of sufficient explanations. As the exact computation is intractable, we described a modular algorithm for computing approximate explanations using a *causal ranking* of parts of the input image, viewing the classifier as a black box. Our experiments demonstrate that an implementation of our algorithm in the tool ReX produces results that are superior to those of state-of-the-art tools according to standard measures.

In the future, we will apply ReX to other modalities that lend themselves to occlusion-based reasoning, such as tabular data, time series, spectroscopy, etc. We will also explore different domains of application, where precise explanations are instrumental, in particular mission-critical and safety-critical domains, such as the healthcare AI and autonomous vehicles. The healthcare domain will require some adaptations of our algorithms, since the quality of medical images is different from the quality of general images (e.g., there are fewer colors in an X-ray than in a general image). In the automotive domain, we will adapt ReX to analyze object detectors and also devise new algorithms that work in (near) real-time, to address the needs of explainability for autonomous vehicles.

## References

- Adebayo, J.; Gilmer, J.; Muelly, M.; Goodfellow, I.; Hardt, M.; and Kim, B. 2018. Sanity checks for saliency maps. In *Proceedings of the 32nd International Conference on Neural Information Processing Systems, NIPS’18*, 9525–9536. Red Hook, NY, USA: Curran Associates Inc.
- Beckers, S. 2021. Causal sufficiency and actual causation. *Journal of Philosophical Logic* 50:1341–1374.
- Blake, N.; Chockler, H.; Kelly, D. A.; Pena, S. C.; and Chanchal, A. 2023. Mrxai: Black-box explainability for image classifiers in a medical setting. *arXiv preprint arXiv:2311.14471*.
- Calderón-Peña, S.; Chockler, H.; and Kelly, D. A. 2024. Real-time incremental explanations for object detectors. *arXiv preprint arXiv:2408.11963*.
- Chajewska, U., and Halpern, J. Y. 1997. Defining explanation in probabilistic systems. In *Uncertainty in Artificial Intelligence (UAI)*, 62–71. Morgan Kaufmann.
- Chen, J.; Song, L.; Wainwright, M.; and Jordan, M. 2018. Learning to explain: An information-theoretic perspective on model interpretation. In *International Conference on Machine Learning (ICML)*, volume 80, 882–891. PMLR.
- Chockler, H., and Halpern, J. Y. 2024. Explaining image classifiers. In *Proceedings of the 21st International Conference on Principles of Knowledge Representation and Reasoning, KR*.

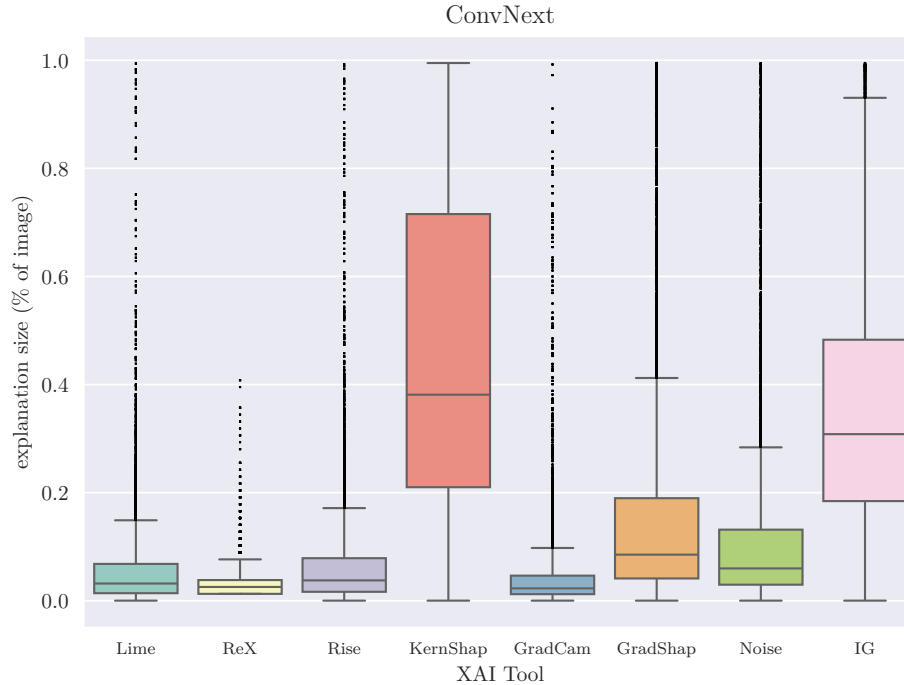


Figure 10: Box plot of all tools over all datasets with a ConvNext model. ReX has the lowest median value and also the smallest number of outliers. It even outperforms GRAD-CAM, a purely white-box tool.

Chockler, H.; Kelly, D. A.; and Kroening, D. 2023. Multiple different explanations for image classifiers. *arXiv preprint arXiv:2309.14309*.

Datta, A.; Sen, S.; and Zick, Y. 2016. Algorithmic transparency via quantitative input influence: Theory and experiments with learning systems. In *Security and Privacy (S&P)*, 598–617. IEEE.

Eiter, T., and Lukasiewicz, T. 2002. Complexity results for structure-based causality. *Artif. Intell.* 142(1):53–89.

Eiter, T., and Lukasiewicz, T. 2004. Complexity results for explanations in the structural-model approach. *Artif. Intell.* 154(1-2):145–198.

Everingham, M.; Van Gool, L.; Williams, C. K. I.; Winn, J.; and Zisserman, A. The PASCAL Visual Object Classes Challenge 2012 (VOC2012) Results. <http://www.pascal-network.org/challenges/VOC/voc2012/workshop/index.html>.

Fong, R.; Patrick, M.; and Vedaldi, A. 2019. Understanding deep networks via extremal perturbations and smooth masks. In *International Conference on Computer Vision (ICCV)*, 2950–2958. IEEE.

Gärdenfors, P. 1988. *Knowledge in Flux*. MIT Press.

Glymour, C., and Wimberly, F. 2007. Actual causes and thought experiments. In Campbell, J.; O’Rourke, M.; and Silverstein, H., eds., *Causation and Explanation*. Cambridge, MA: MIT Press. 43–67.

Hall, N. 2007. Structural equations and causation. *Philosophical Studies* 132:109–136.

Halpern, J. Y., and Pearl, J. 2005a. Causes and explanations: a structural-model approach. Part I: causes. *British Journal for Philosophy of Science* 56(4):843–887.

Halpern, J. Y., and Pearl, J. 2005b. Causes and explanations: A structural-model approach. Part I: Causes. *British Journal for the Philosophy of Science* 56(4).

Halpern, J. Y., and Pearl, J. 2005c. Causes and explanations: A structural-model approach. Part II: Explanations. *British Journal for the Philosophy of Science* 56(4).

Halpern, J. Y. 2019. *Actual Causality*. The MIT Press.

Hempel, C. G. 1965. *Aspects of Scientific Explanation*. Free Press.

Hitchcock, C. 2001. The intransitivity of causation revealed in equations and graphs. *Journal of Philosophy* XCVIII(6):273–299.

Hitchcock, C. 2007. Prevention, preemption, and the principle of sufficient reason. *Philosophical Review* 116:495–532.

Kokhlikyan, N.; Miglani, V.; Martin, M.; Wang, E.; Alsallakh, B.; Reynolds, J.; Melnikov, A.; Kliushkina, N.; Araya, C.; Yan, S.; and Reblitz-Richardson, O. 2020. Captum: A unified and generic model interpretability library for PyTorch. *arXiv*.

Lundberg, S. M., and Lee, S.-I. 2017a. A unified approach to interpreting model predictions. In *Advances in Neural In-*

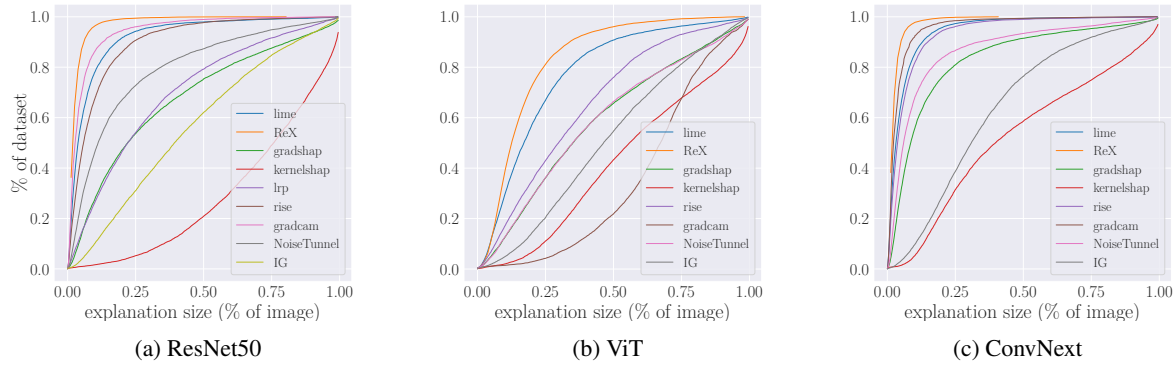


Figure 11: Cumulative plots of explanations sizes with 3 different models over all datasets. ReX consistently produces smaller explanations, meaning it identifies precisely those pixels required for the classification, with fewer unnecessary pixels.

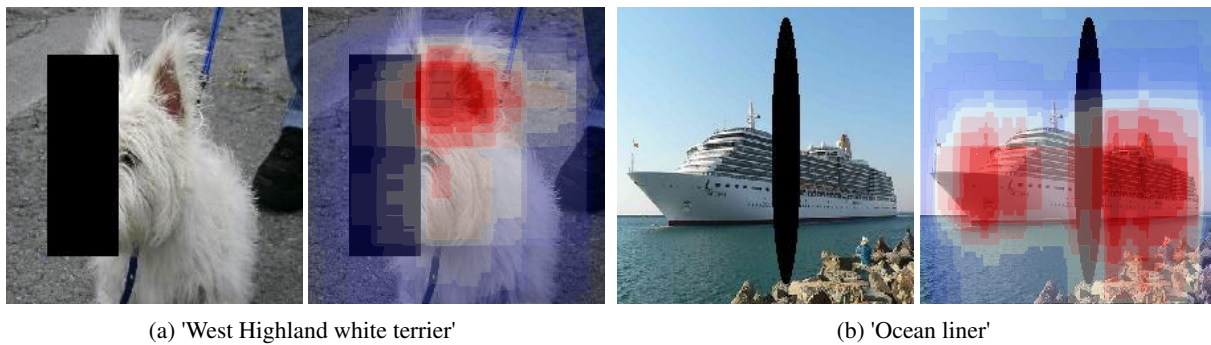


Figure 12: Photo Bombing images and output from ReX

formation Processing Systems (*NeurIPS*), volume 30, 4765–4774.

Lundberg, S. M., and Lee, S.-I. 2017b. A unified approach to interpreting model predictions. In Guyon, I.; Luxburg, U. V.; Bengio, S.; Wallach, H.; Fergus, R.; Vishwanathan, S.; and Garnett, R., eds., *Advances in Neural Information Processing Systems*, volume 30. Curran Associates, Inc.

Pearl, J. 1988. *Probabilistic Reasoning in Intelligent Systems*. Morgan Kaufmann.

Petsiuk, V.; Das, A.; and Saenko, K. 2018. RISE: randomized input sampling for explanation of black-box models. In *British Machine Vision Conference (BMVC)*. BMVA Press.

Ribeiro, M. T.; Singh, S.; and Guestrin, C. 2016. “Why should I trust you?” Explaining the predictions of any classifier. In *Knowledge Discovery and Data Mining (KDD)*, 1135–1144. ACM.

Russakovsky, O.; Deng, J.; Su, H.; Krause, J.; Satheesh, S.; Ma, S.; Huang, Z.; Karpathy, A.; Khosla, A.; Bernstein, M.; Berg, A. C.; and Fei-Fei, L. 2015. ImageNet Large Scale Visual Recognition Challenge. *International Journal of Computer Vision (IJCV)* 115(3):211–252.

Salmon, W. C. 1989. *Four Decades of Scientific Explanation*. University of Minnesota Press.

Selvaraju, R. R.; Cogswell, M.; Das, A.; Vedantam, R.;

Parikh, D.; and Batra, D. 2017. Grad-CAM: Visual explanations from deep networks via gradient-based localization. In *International Conference on Computer Vision (ICCV)*, 618–626. IEEE.

Shi, J.; Yan, Q.; Xu, L.; and Jia, J. 2016. Hierarchical image saliency detection on extended cssd. *IEEE Transactions on Pattern Analysis and Machine Intelligence* 38(4):717–729.

Shitole, V.; Li, F.; Kahng, M.; Tadepalli, P.; and Fern, A. 2021. One explanation is not enough: Structured attention graphs for image classification. In *Neural Information Processing Systems (NeurIPS)*, 11352–11363.

Shrikumar, A.; Greenside, P.; and Kundaje, A. 2017. Learning important features through propagating activation differences. In *ICML*, volume 70, 3145–3153. JMLR.org.

Smilkov, D.; Thorat, N.; Kim, B.; Viégas, F.; and Wattenberg, M. 2017. SmoothGrad: removing noise by adding noise. *arXiv*.

Springenberg, J. T.; Dosovitskiy, A.; Brox, T.; and Riedmiller, M. A. 2015. Striving for simplicity: The all convolutional net. In *ICLR (Workshop Track)*.

Sun, Y.; Chockler, H.; Huang, X.; and Kroening, D. 2020. Explaining image classifiers using statistical fault localization. In *ECCV, Part XXVIII*, volume 12373 of *LNCS*, 391–406. Springer.

Sundararajan, M.; Taly, A.; and Yan, Q. 2017. Axiomatic attribution for deep networks. In *International Conference on Machine Learning*, 3319–3328. PMLR.

Weslake, B. 2015. A partial theory of actual causation. *British Journal for the Philosophy of Science* To appear.

Woodward, J. 2003. *Making Things Happen: A Theory of Causal Explanation*. Oxford, U.K.: Oxford University Press.